Multiplexed peroxidase-based electron microscopy labeling enables simultaneous visualization of multiple cell types

Qiyu Zhang[1,2], **Wei-Chung A. Lee**[3], **David L. Paul**[1,*], and **David D. Ginty**[1,2,*]

[1]Department of Neurobiology, Harvard Medical School, Boston, Massachusetts, United States 02115

[2]Howard Hughes Medical Institute, Harvard Medical School, Boston, Massachusetts, United States 02115

[3]F.M. Kirby Neurobiology Center, Boston Children's Hospital, Boston, Massachusetts, United States 02115

Abstract

Electron microscopy (EM) is a powerful tool for circuit mapping, but identifying specific cell types in EM datasets remains a major challenge. Here we describe a technique enabling simultaneous visualization of multiple, genetically identified neuronal populations so that synaptic interactions between them can be unequivocally defined. We present 15 AAV constructs and six mouse reporter lines for multiplexed EM labeling in the mammalian nervous system. These reporters feature dAPEX2, which exhibits dramatically improved signal compared to previously described ascorbate peroxidases. By targeting this enhanced peroxidase to different subcellular compartments, multiple orthogonal reporters can be simultaneously visualized and distinguished under EM using a protocol compatible with existing EM pipelines. Proof-of-principle double and triple EM labeling experiments demonstrated synaptic connections between primary afferents, descending cortical inputs, and inhibitory interneurons in the spinal cord dorsal horn. Our multiplexed peroxidase-based EM labeling system should therefore greatly facilitate analysis of connectivity in the nervous system.

Introduction

Precise patterns of synaptic connectivity are central to nervous system function, and thus a major ongoing effort of neuroscience research is defining detailed maps of synaptic interactions throughout the nervous system. Currently, the main strategies for visualizing synaptic connectivity rely on light microscopy (LM) and electron microscopy (EM). With

advances in molecular genetic approaches, specific neurons and their synapses can be genetically labeled for visualization using both microscopic approaches. However, while multiplexed labeling strategies are readily implemented in LM, a practical system for multiplexed labeling in EM is not available. Thus, it has not been possible to fully combine the power of molecular genetics with EM, which could greatly facilitate efforts towards defining patterns of synaptic connectivity in the nervous system.

Several LM techniques have been developed to investigate synaptic connections between different neuronal populations. With fluorescence microscopy, spectrally separated fluorescent proteins can be localized to pre- or postsynaptic structures to identify synaptic partners[1, 2], and more complex approaches such as GRASP, where signals are only detected at synapses with both pre- and postsynaptic partners expressing specific marker proteins, have also been developed[3, 4]. However, the resolution of LM is limited by diffraction, and the sizes of synaptic structures are typically below the LM resolution limit. Recently, super-resolution microscopy[5] and expansion microscopy[6] have been used to address this problem, however achieving the resolution necessary for visualizing fine neurites and synaptic structures is not always possible. Furthermore, fluorescence-based LM methods selectively label particular proteins; surrounding, unlabeled neuropil and intracellular compartments are not visible. Thus, many important contextual details relevant to neuronal circuitry are discarded.

EM remains the only unbiased method for comprehensively resolving the different components of synapses and structurally identifying synaptic partners. Recent advances in EM sectioning and imaging methods have made large-scale reconstructions and connectomics possible, leading to the generation of comprehensive maps of synaptic connectivity[7–10]. Despite these major advances, EM-derived connectome data can be difficult to place into a functional context because the molecular and physiological identities of pre- and postsynaptic partners generally cannot be determined. Long-range projection neurons whose axons can span nearly the entire body suffer particularly from this issue as they are particularly difficult to trace across many sections. For EM visualization, approaches using genetically expressed peroxidases and miniSOG afford a powerful strategy to label defined neuronal populations, including projection neurons, providing identity information for one of the two synaptic partners[11–16]. A greater challenge, however, is to simultaneously label multiple defined neuronal populations for EM analysis, which is necessary to establish the identities of pre- and postsynaptic partners as well as the convergence of multiple synapses onto common targets. Unlike fluorescence microscopy, commonly used EM imaging techniques do not permit multiplexed labeling by spectral separation. In single sections, this issue could be addressed with immuno-EM or energy-filtered transmission EM (EFTEM) with spectral resolution[17]; in volumes created from serial images, this could be addressed with correlated light and electron microscopy (CLEM) using multiple fluorescence channels, and recent advances allow high-accuracy tracking of single axons[18] and immunostaining with ultrastructural preservation[19]. However, a technique that works well with both single sections and volumes that is versatile and simple to implement is still lacking.

To circumvent this technical challenge, we have developed tools for double, triple and higher order EM labeling by targeting peroxidase reporters to distinct cellular compartments. A previous report using double peroxidase labeling in *Drosophila* successfully enabled simultaneous visualization of two labeled cell types, however synaptic ultrastructure could not be visualized in this previous report and therefore synapse identification was not possible[20]. The multiplexed EM labeling strategy reported here works exceptionally well with conventional EM pipelines with minimal modification, and provides simultaneous, unequivocal identification of pre- and postsynaptic neurons in EM volumes. We report the generation of a multiplexed EM labeling toolkit comprised of single Cre-recombinase-dependent, Flp-recombinase-dependent, and Cre-and-Flp-dual-recombinase-dependent mouse lines, as well as an array of adeno-associated virus (AAV) vectors that allow versatile multiplexed EM labeling. This multiplexed EM labeling toolkit should facilitate efforts to define patterns of synaptic connectivity throughout the mammalian nervous system.

Results

Optimization of a peroxidase for EM labeling in the mammalian nervous system

To explore the suitability of peroxidases for multiplexed EM labeling of neurons in mice, we began by testing previously described peroxidase reporter constructs (Supplementary Table 1). We first focused on defining ultrastructural features and synaptic partners of primary somatosensory neurons, whose cell bodies reside in dorsal root ganglia (DRG) and axonal projections extend peripherally into the skin and internal organs, and centrally into the spinal cord and brainstem. DRG neurons could be efficiently transduced (>90%) by neonatal AAV9 intraperitoneal (IP) injection, with small-diameter DRG neurons generally expressing AAV-delivered transgenes at higher levels than large-diameter neurons[21] (Supplementary Fig. 1). A small number of spinal cord and cortical neurons were also transduced (data not shown). While two previously described plasma membrane-targeted horseradish peroxidase (HRP) constructs, HRP-TM[22] and mHRP[12], labeled the membranes of transduced HEK293T cells (HRP-TM shown in Supplementary Fig. 2a, b), neither resulted in detectable staining of DRG axonal projections within the spinal cord following AAV9 delivery via IP injection (data not shown). Moreover, injections of the same constructs with the AAV1 capsid into the neocortex resulted in expression levels detectable by LM (Supplementary Fig. 2c), but surprisingly failed to yield detectable labeling by EM (Supplementary Fig. 2d). We speculate that the discrepancy occurred because the LM signal reflects the summation of staining throughout a thick vibratome section, but the staining was too diffuse to be visualized in EM of a single ultrathin section. A plasma membrane-targeted HRP construct, HRP-DsRed-GPI[20, 23], which worked well in *Drosophila* neurons, failed to traffic to the plasma membrane of cells in mouse cortex (data not shown). A construct targeting synaptic vesicles, VAMP2-HRP[11], which could be visualized in mouse hypothalamic neurons, labeled only one or two vesicles per terminal under the fixation and sample preparation conditions used in conventional EM pipelines. We also tested constructs expressing APEX2, an enhanced soybean ascorbate peroxidase (APX) that is less catalytically active than HRP, but is functional when expressed in cytosolic environments, unlike HRP[24]. After transduction of neonatal DRG neurons by IP injection of AAV9 containing a mitochondrial-matrix-targeted APEX2 construct, mito-V5-APEX2[25], transverse spinal cord sections were

stained for peroxidase activity. Axons of small-diameter neurons, which terminate in superficial laminae of the spinal cord dorsal horn, were strongly labeled (Fig. 1a, black arrow), but axons of large-diameter neurons, which terminate in deeper laminae, exhibited low or undetectable labeling. The poor labeling of DRG axon terminals in the deep dorsal horn was not due to lack of transduction or failure of mito-V5-APEX2 expression in large-diameter DRG neurons, as mitochondrial labeling of both large- and small-diameter neuronal somata in the DRG was observed (data not shown). One possible explanation for the lack of deep dorsal horn staining is the relatively lower expression levels in the large-diameter neurons. Taken together, these results indicate that the performance of existing peroxidase constructs is strongly influenced by differences in the systems used for testing, including cell type, species of origin of those cells and sample preparation methods. Therefore, we attempted to optimize reporters and labeling conditions to visualize long-range axon projections for ultrastructural synaptic analyses in mice.

In the process of creating APEX2 from APX, two residues (K14 and E112) at the dimeric interface were mutated to increase monomericity, thereby avoiding the concern that incorporation of a dimerizing peroxidase into a fusion protein could potentially induce mislocalization or alter function in an unexpected way[24, 26]. However, the mutations also decreased signal levels in tissue culture cells, possibly from lowered heme affinity and thermal stability[24, 26]. We reasoned that dimerization of APEX2 should not be problematic to achieve our goal of directing peroxidase reporters to different subcellular compartments. Thus, we introduced the native residues to the dimeric interface of APEX2, presumably enhancing heme affinity and thermal stability, and designated the resultant protein dAPEX2, for dimeric APEX2, although dimerization was not directly tested. Matrix-dAPEX2, which has the same sequence as mito-V5-APEX2 except for the replacement of APEX2 with dAPEX2, was packaged into AAV9 and used for IP injection to test its activity. We found that Matrix-dAPEX2 exhibits substantially increased staining intensity (Fig. 1b) compared to mito-V5-APEX2 (Fig. 1a). The dorsal horn was intensely and evenly stained along the dorsoventral axis with Matrix-dAPEX2, mirroring the efficiency of DRG somata labeling. Axons containing labeled mitochondria (Fig. 1c, red arrows) in the dorsal horn could be clearly visualized in EM and easily distinguished from those containing unlabeled mitochondria (Fig. 1c, blue arrows). We also systematically investigated peroxidase reaction conditions and sample preparation strategies to determine optimal procedures for detecting the dAPEX2 catalyzed reaction product by EM (see Methods and Supplementary Fig. 3–5). These simple, optimized conditions do not require detergent extraction of the sample and include concentrations of glutaraldehyde appropriate for excellent specimen preservation, allowing dAPEX2 to be used for investigating the ultrastructural properties of labeled neurons and their long-range projections.

Mitochondria are ideal for EM labeling in neurons because they are abundant in somata, dendrites, axons and axon terminals. In addition, ultrastructural details of mitochondrial-labeled cells are more clearly visualized than those of cells labeled with a cytosolic reporter, because the spread of the peroxidase reaction product is limited by the mitochondrial membrane. This feature is crucial when ultrastructural details such as cytosolic electron density and synaptic vesicle morphology are of interest. To test the utility of EM labeling of long-range projection neurons using Matrix-dAPEX2, we performed cortical injections of a

Cre-dependent AAV1-DIO-Matrix-dAPEX2 into the Tg(Rbp4-Cre)KL100 mouse line, which restricts expression to cortical layer 5 pyramidal tract and inter-telencephalic corticofugal neurons[27]. Robust labeling was observed in the cell body (Fig. 1d, left panel), dendrites (Fig. 1d, middle panel) and corticospinal terminals in the dorsal horn of the cervical spinal cord (Fig. 1d, right panel). We also applied Matrix-dAPEX2 labeling to a previously intractable problem: defining the ultrastructural properties of physiologically distinct populations of small-diameter, unmyelinated primary somatosensory neuronal axons, also known as C-fibers. These small-diameter neurons include nociceptors, thermoceptors, pruriceptors, and a subset of low-threshold mechanoreceptors (LTMRs)[28]. Peripheral terminals of these subtypes are morphologically distinct[28] but no structural difference in their central terminations have been described. Due to the fine caliber of C-fibers, adequate filling of these small-diameter neurons with HRP through recording pipettes to visualize their axonal projections to the spinal cord or periphery has proven to be a major challenge[29, 30]. To label select populations of C-fibers, Cre-dependent AAV9-DIO-Matrix-dAPEX2 was injected IP into $Th^{T2A\text{-}CreER}$[31], $Mrgprd^{Cre}$[32], and $Mrgprb4^{Cre}$[33] mouse lines, which express CreER or Cre recombinase in three physiologically distinct nonpeptidergic C-fiber subtypes: C-LTMRs, Mrgprd$^+$ polymodal nociceptors, and Mrgprb4$^+$ afferents implicated in tactile sensation, respectively. This strategy allowed robust labeling of these different C-fiber populations, as indicated by LM (Fig. 1e, g, i) and EM (Fig. 1f, h, j) peroxidase labeling patterns. EM analysis in the spinal cord showed that each of the three classes of primary sensory neurons often forms synapses onto multiple postsynaptic dendrites (Fig. 1f, h, j, arrowheads), as the labeled axons (Fig. 1f, h, j, asterisks) were observed in complexes termed synaptic glomeruli[34]. Moreover, the terminals of each sensory neuron class receive abundant axoaxonic connections. Because the peroxidase reporter is confined to the mitochondrial matrix, we were able to observe ultrastructural differences that distinguish the axon terminals of the three labeled sensory neuron populations, with synaptic vesicle morphology being the most apparent difference. While C-LTMRs mostly contain round, clear vesicles and lack clusters of vesicles, Mrgprd$^+$ polymodal nociceptors and Mrgprb4$^+$ afferents typically exhibit large, variably shaped dense-core vesicles and clusters of vesicles (Fig. 1f, h, j, green and yellow arrows). Therefore, a recombinase-dependent, mitochondrial-matrix-targeted dAPEX2 AAV construct, used in conjunction with genetic tools to selectively label neuronal subtypes, enables neuronal-subtype-specific visualization of the ultrastructural properties of axonal terminals and their synaptic arrangements by EM.

Simultaneous visualization of multiple genetically defined populations using peroxidase constructs targeted to different subcellular compartments

The finding that targeting dAPEX2 to the mitochondrial matrix can enable comparisons between the synapses of sensory neuron subtypes suggested that simultaneously targeting peroxidases to distinct subcellular compartments in two or more genetically defined neurons would allow for visualization of their synaptic relationships. To generate new peroxidase reporters targeted to distinct subcellular compartments abundant in axons and dendrites for multiplexed EM labeling, we tested dAPEX2 or HRP fused to targeting motifs for the plasma membrane, microtubules, mitochondrial intermembrane space (IMS), peroxisomes, synaptic vesicles (SV), and endoplasmic reticulum (ER) (Supplementary Table 1). These

peroxidase constructs were tested in HEK293T cells and in mice by IP or cortical AAV injections (Supplementary Table 1). This testing yielded four additional constructs useful for multiplexed EM labeling: untagged, soluble dAPEX2, which labels the cytosol and nucleus (Fig. 2a), ER-dAPEX2, which includes an N-terminal Igκ signal sequence and a C-terminal KDEL ER retention sequence and labels the ER (Fig. 2b), IMS-dAPEX2, which contains the localization signal from LACTB and labels the mitochondrial IMS (Fig. 2c), and SV-HRP, a fusion protein of synaptophysin and HRP, which labels the lumen of synaptic vesicles (Fig. 2d). EM signals from dAPEX2, Matrix-dAPEX2, ER-dAPEX2, and IMS-dAPEX2 could be readily observed in neuronal somata, dendrites, and short axons, while SV-HRP could be observed only in axon terminals (in all figures, red arrows indicate labeled structures and blue arrows indicate unlabeled equivalents). Signals from dAPEX2, Matrix-dAPEX2, IMS-dAPEX2 and SV-HRP, but very little from ER-dAPEX2 (data not shown), were also observed in terminals of long-range axonal projections, which in mice can reach several centimeters in length (Fig. 2). In addition to neurons in the cerebral cortex, spinal cord and DRG shown here, some of these constructs were also shown to effectively label neurons in the cerebellum (Laurens Witter, Chong Guo, Wade Regehr, unpublished data) and the hippocampus (Ee-Lynn Yap, Michael Greenberg, unpublished data). It is noteworthy that in any given plasma-membrane-enclosed profile, all mitochondria are either labeled or unlabeled (100.0 ± 0.0%, mean ± SD, n = 30 profiles for both Matrix-dAPEX2 and IMS-dAPEX2), implying that the penetrance for matrix and IMS labeling in transduced cells is 100%, which is useful for registering profiles across different sections. The same is likely true for cytosolic and ER labeling because the cytosol and ER are largely continuous compartments where dAPEX2 can freely diffuse. SV-HRP labeled vesicles constituted 19.6 ± 12.4% (mean ± SD, n = 30 profiles) of the total synaptic vesicles in labeled presynaptic profiles. Expression of these constructs did not lead to increased mortality, or gross behavioral, anatomical or cytological abnormalities, with the exception of IMS-dAPEX2, which induced mitochondrial aggregation when expressed at very high levels but not at the levels employed in this study (see Supplementary Table 1). Therefore, these five orthogonal dAPEX2 and HRP constructs are excellent candidates for further development of a multiplexed EM labeling system for mice.

To simultaneously label multiple genetically defined neuronal populations for synapse analysis, we used orthogonal expression systems. Currently, Cre, Flp and Dre recombinases, as well as transcription factors such as tTA/rtTA are used for directed expression of reporter genes in mice, with Cre and Flp recombinases being most widely used. Specific neuronal populations can also be targeted anatomically using AAV injections or by taking advantage of the different tropisms of AAV capsids[35]. Therefore, we constructed constitutively expressed as well as Cre- and Flp-recombinase-dependent AAV vectors for dAPEX2, Matrix-dAPEX2, ER-dAPEX2, IMS-dAPEX2, and SV-HRP (Table 1). To address the utility of these AAV constructs for multiplexed EM labeling, we employed two different genetic strategies. For the first strategy, we crossed the Tg(Rbp4-Cre)KL100 mouse line with the $Pvalb^{T2A-FlpO}$ line, which expresses FlpO in fast spiking cortical interneurons, including basket and chandelier cells[36]. We performed cortical injections of Cre-dependent AAV1-DIO-ER-dAPEX2 and Flp-dependent AAV1-FDIO-Matrix-dAPEX2 into Tg(Rbp4-Cre)KL100; $Pvalb^{T2A-FlpO}$ neonates. Cells with ER labeling (Fig. 3a, red asterisks) and

mitochondrial matrix labeling (Fig. 3a, green asterisks) were easily observed and distinguished, and since neither dAPEX2 reporter obscures ultrastructural details, identification of synapses was straightforward. EM analysis revealed Pvalb[+] neuron to Rbp4^{+} neuron synapses that were typically perisomatic and symmetric (Fig. 3a, arrowheads), consistent with prior electrophysiological and EM studies[37]. For a second test, we used *Slc32a1*[IRES-Cre] mice, in which Cre is expressed in all inhibitory neurons[38], and *Avil*[FlpO] mice, in which FlpO is expressed in all primary somatosensory neurons (Ling Bai, D.D.G., unpublished data). AAV9-FDIO-IMS-dAPEX2 was delivered by IP injection into *Slc32a1*[IRES-Cre]; *Avil*[FlpO] neonates followed by a dorsal horn injection of AAV1-DIO-Matrix-dAPEX2 at P11-P12. This resulted in robust labeling of dorsal horn inhibitory interneurons, identified by peroxidase staining of their mitochondrial matrix (Fig. 3b, red asterisks), and somatosensory neuron terminals, identified by staining of their mitochondrial IMS (Fig. 3b, green asterisks). In this case, axodendritic synapses from primary afferents onto dorsal horn inhibitory interneurons and axoaxonic synapses from inhibitory interneurons onto primary afferents were readily seen (Fig. 3b, arrowheads). The latter type of synapse is believed to underlie presynaptic inhibition, an important mechanism for central control of somatosensory input[39].

To address the feasibility of simultaneously labeling three neuronal populations, we used *Slc32a1*[IRES-Cre]; *Avil*[FlpO] mice, and injected AAV9-FDIO-IMS-dAPEX2 IP to label primary afferents, AAV1-DIO-ER-dAPEX2 into the dorsal horn to label spinal cord inhibitory interneurons, and AAV1-Matrix-dAPEX2 into the cortex to label descending corticospinal neurons. Each of the three labeled structures, ER (Fig. 3c, red asterisks), mitochondrial IMS (Fig. 3c, green asterisks), and mitochondrial matrix (Fig. 3c, blue asterisks), respectively, were clearly visualized and distinguished from the other two structures in the spinal cord dorsal horn by EM. Consistent with previous reports[34, 40], primary afferents (green asterisks) often form glomerular synapses, while corticospinal axons (blue asterisks) mainly form simple synaptic interactions. In addition, inhibitory interneurons (red asterisks) represent a large fraction of all postsynaptic partners for both types of long-range inputs into the dorsal horn.

In order to investigate whether these reporters can be used for multiple labeling in volume EM, we serially sectioned one of the spinal cord dorsal horn samples used for Fig. 3b, and imaged a volume of $35 \times 24 \times 2$ μm. These two labels could be readily seen throughout the volume and did not cause any issue in montaging or alignment. We used this volume to reconstruct a primary afferent (green) and two inhibitory interneuron profiles (axon in light red and dendrite in dark red) where synaptic interactions were seen (Fig. 4a, b and Supplementary Video 1 and 2). We also determined the discriminability of the two mitochondrial labels using this image volume. Two annotators independently categorized all the mitochondria as either matrix-labeled, IMS-labeled, or unlabeled in a volume of $12 \times 8 \times 2$ μm, and then the annotations were compared. Of the 325 mitochondria annotated, 319 had matching annotations (98.2%), and only six mitochondria had mismatching annotations (1.8%) (Fig. 4c). Of the six mismatching annotations, one was a matrix-labeled vs. IMS-labeled mismatch, one was a matrix-labeled vs. unlabeled mismatch, and four were IMS-labeled vs. unlabeled mismatches. Three of the IMS-labeled vs. unlabeled mismatches resulted from human error during annotation. This indicates that the two mitochondrial

labels are readily distinguishable from each other. Because the three other orthogonal labels are targeted to different organelles, they are even more easily distinguished from each other and the two mitochondrial labels, and the few mismatches for the volume annotated here for mitochondrial matrix vs. mitochondrial IMS thus likely represents a worst-case scenario.

Therefore, labeling with orthogonal EM reporters provides a versatile approach to investigate complex synaptic interactions in both single sections and volumes. In all, the fifteen AAV peroxidase reporter constructs (Table 1), used with orthogonal recombinase-dependent expression systems and anatomically defined injections, allow simultaneous double, triple, and possibly higher order EM labeling to visualize and define synaptic arrangements in complex neuropils.

Generation and characterization of mouse lines encoding orthogonal EM reporters

To complement the use of the AAV peroxidase reporter constructs and increase the versatility of the multiplexed peroxidase EM labeling strategy, we next generated mouse lines that conditionally express two of the dAPEX2 reporters. These mouse reporter lines can be used in conjunction with the AAV peroxidase reporter vectors for multiplexed EM labeling, and for many applications will be preferable to AAV vectors. For example, mouse reporter lines may be superior if: 1) AAVs lead to variable levels of expression due to variability of transduction; 2) recombinases must be expressed during embryonic development to successfully label a particular neuronal type; or 3) complex surgeries are required to inject AAVs into target regions, which may be technically challenging or result in tissue damage. Thus, mouse lines that conditionally express dAPEX2 reporters in defined neuronal subtypes should enable a diverse range of single or multiplexed EM labeling applications.

We first generated Cre- and Flp-dual-recombinase-dependent reporter lines for both Matrix-dAPEX2 and ER-dAPEX2 (Fig. 5a). The targeting strategy employed a dual-recombinase-dependent expression cassette with an artificial CAG promoter[36] preceding the dAPEX2 reporters knocked into the *Gt(ROSA)26Sor* (*ROSA26*) locus for ubiquitous tissue expression. The frt-STOP-frt and loxP-STOP-loxP cassettes enable Flp- and Cre-dependent expression, respectively[36]. Mice carrying these knock-in alleles, termed *ROSA26^DR-Matrix-dAPEX2^* and *ROSA26^DR-ER-dAPEX2^*, were generated and tested for recombinase-dependent reporter expression by cortical injection of AAV1-Cre, AAV1-FlpO, or a mixture of both. AAV1-tdTomato was co-injected to mark the injection site and evaluate viral transduction. We found no peroxidase activity from dAPEX2 in the cortex of mice injected with AAVs lacking recombinases, AAV1-Cre alone, or AAV1-FlpO alone (Fig. 5b, c, left three panels), demonstrating tight control of reporter expression by each of the STOP cassettes. On the other hand, co-injection of AAV1-Cre and AAV1-FlpO resulted in strong peroxidase activity from dAPEX2 in the brains of *ROSA26^DR-Matrix-dAPEX2^* and *ROSA26^DR-ER-dAPEX2^* mice (Fig. 5b, c, rightmost panel), demonstrating high recombinase-dependent dAPEX2 expression from both reporter lines. Subsequently, single-recombinase-dependent reporter lines were generated by germline deletion of the appropriate STOP cassettes (Table 2). To determine whether dAPEX2 peroxidase levels in these mouse lines are sufficient for EM identification of labeled neurons, we prepared dual AAV-transduced

cortical samples for EM analysis. Ultrathin sections revealed easily identifiable, correctly localized staining in both $ROSA26^{DR\text{-}Matrix\text{-}dAPEX2}$ (Fig. 5d) and $ROSA26^{DR\text{-}ER\text{-}dAPEX2}$ (Fig. 5e) mice.

Since labeling many neuronal populations and their projections requires intersectional genetic strategies, we investigated whether the $ROSA26^{DR\text{-}Matrix\text{-}dAPEX2}$ line can label long-range axonal projections in a dual-recombinase-dependent manner using mouse recombinase driver lines. For this, we generated $Scn10a^{Cre}$; $Avil^{FlpO}$; $ROSA26^{DR\text{-}Matrix\text{-}dAPEX2}$ animals: $Scn10a^{Cre}$ expresses Cre recombinase in virtually all C-fiber sensory neurons and a smaller number of medium-diameter lightly myelinated sensory neurons[41, 42], and $Avil^{FlpO}$ expresses FlpO recombinase in all somatosensory neurons. By LM, strong staining in the superficial dorsal horn, as well as sparse labeling in the deep dorsal horn and dorsal column was observed, while no labeling of spinal cord neurons or the corticospinal tract was observed, as predicted (Fig. 6a, left panel). By EM, abundant labeled axon terminals (red asterisks) were observed in the superficial laminae of the dorsal horn (Fig. 6a, middle panel), as well as some myelinated axons and axon terminals in deeper laminae (Fig. 6a, right panel). Axon terminals of these long-range projection neurons could also be observed in the skin with LM (Fig. 6b, left panel), and labeled longitudinal lanceolate endings associated with hair follicles (Fig. 6b, middle panel) and free nerve endings (Fig. 6b, right panel) within the epidermis were seen under EM. We also tested whether C-LTMRs could be selectively labeled using this reporter line by generating $Th^{T2A\text{-}CreER}$; $Avil^{FlpO}$; $ROSA26^{DR\text{-}Matrix\text{-}dAPEX2}$ animals. Indeed, similar staining patterns could be seen under LM as in Fig. 1e (data not shown). Additionally, labeled axonal profiles with similar ultrastructure to those shown in Fig. 1f were observed under EM (Fig. 6c). These findings demonstrate that the $ROSA26^{DR\text{-}Matrix\text{-}dAPEX2}$ mouse line works well for labeling long-range projections of genetically defined neuronal populations. Finally, we generated mice harboring the $Slc32a1^{IRES\text{-}Cre}$ and Cre-dependent $ROSA26^{LSL\text{-}ER\text{-}dAPEX2}$ alleles to label the ER in inhibitory interneurons throughout the nervous system. We observed correctly localized ER labeling in inhibitory neurons in cortex, spinal cord dorsal horn, and striatum, demonstrating the wide range of brain regions and neurons that could be visualized using this mouse line (Fig. 6d).

Discussion

Here we describe a multiplexed peroxidase-based labeling strategy for simultaneous visualization of multiple neuronal populations by EM. We also report six new dAPEX2 mouse reporter lines and 15 AAV peroxidase constructs that comprise a versatile toolkit for multiplexed labeling. These tools, which have been deposited into public repositories, can be used alone or in combination to define synaptic arrangements of complex neuropils in mammalian systems.

Historically, multiplexed labeling in EM has been a major challenge. One approach to multiplexed EM labeling is to use antibodies conjugated with different-sized gold particles for immuno-EM. While immuno-EM is valuable for providing information on protein localization, it is difficult to implement because many, if not most, epitopes are destroyed or rendered inaccessible by conventional EM specimen preparation. Furthermore, specimen

preparations amenable to immuno-EM are poorly suited for preserving the ultrastructural details needed to identify pre- and postsynaptic structures. A more recent approach using EFTEM to achieve spectral separation for different stains, requires highly specialized equipment and long exposure times[17], and is unlikely to be feasible for most applications including large-scale reconstructions. CLEM has also been used to identify multiple neuronal populations in tissue volumes. Newly developed algorithms have enabled improved accuracy and allowed tracking projection axons in dense neuropils with multiple channels[18]. However, for small profiles such as axons, a relatively large EM volume (encompassing axonal lengths of 40-50 μm) and considerable amount of reconstruction at both LM and EM levels are required for the registration algorithms to identify matching profiles. This approach is time- and labor-intensive and cannot be performed routinely like single-section EM.

Our peroxidase-based multiplexed EM labeling tools take advantage of the simple fact that peroxidase staining can be restricted to distinct cellular compartments and thus the majority of peroxidase reporters we described do not obscure ultrastructural features of cells such as synaptic vesicles, postsynaptic densities, and the cytoskeleton. These peroxidase reporters can be targeted to two, three, four or more cellular compartments, in different populations simultaneously, to address synaptic relationships between genetically defined neuronal populations. An additional key advantage of this approach is that minimal modifications to existing EM pipelines are required for implementation. Thus, in addition to single-section and serial-section transmission EM used here, multiplexed peroxidase EM labeling should also be compatible with serial block-face scanning EM, serial-section scanning EM, focused ion beam scanning EM, and X-ray microscopy[14, 43].

While previously reported peroxidase constructs have been shown to work well in tissue culture and in certain organisms, our findings suggest that many of these are not optimal for the mammalian nervous system. dAPEX2, described here, is more sensitive than APEX2 and can be used in any context where dimerization is tolerated. The improvement on peroxidase activity afforded by dAPEX2 proved critical for the generation of mouse reporter lines, in part because the commonly used ROSA26-CAG cassette typically expresses transgenes at lower levels than viral transduction methods with a concomitant reduction in the level of detection of genetically encoded reporters[1].

The suite of peroxidase EM reporter constructs described here is highly versatile, and may be further increased by generating Dre-dependent and tTA-dependent dAPEX2 and HRP constructs for additional orthogonal driver channels, as well as constructing G-rabies for trans-synaptic tracing. One exciting prospect will be to use the AAV and mouse line EM reporters with serial-section EM to obtain large-scale volume reconstructions for connectomics. Multiplexed EM labeling will reduce costs and efforts for data collection compared to approaches where each desired population is individually labeled, one-by-one, which requires collecting multiple datasets. In addition, the high penetrance of these reporters should facilitate the reconstruction process itself by providing a strong indicator of continuity between profiles in cases where intervening EM sections are omitted or lost. It is likely that more efficient reconstruction algorithms can be developed based on peroxidase labeling. Another potentially valuable use of these peroxidase reporters is functional CLEM.

Previous studies used fluorescent calcium indicators *in vivo* to assess functional properties of neurons and then identified their synaptic connections ultrastructurally[44–46]. One could envision multicolor *in vivo* calcium imaging of different neuronal populations, while using orthogonal peroxidase labeling to identify these neuronal populations in EM, through the use of bicistronic vectors such as Matrix-dAPEX2-IRES-jGCaMP7s and ER-dAPEX2-IRES-jRGECO1a. In all, the 15 AAV constructs and six mouse reporter lines reported here for multiplexed EM labeling in the mammalian nervous system will enable advances in synaptic connectivity mapping with unequivocal genetic identification of synaptic partners.

Methods

All experiments using animals were conducted according to United States National Institutes of Health guidelines for animal research and were approved by the Institutional Animal Care and Use Committee at Harvard Medical School. All procedures were done at room temperature unless otherwise noted.

No statistical methods were used to pre-determine sample sizes but sample sizes are similar to those reported in previous publications (ref. 11). Sample assignment was not randomized. Data collection and analysis were not performed blind to the conditions of the experiments. All materials are available upon request.

Molecular cloning

DNA fragments were synthesized as IDT gBlocks Gene Fragments and/or oligonucleotides and amplified by PCR using Q5 Hot Start (New England Biolabs), and cloned into an AAV expression vector (Addgene plasmid # 20299) using In-Fusion HD (Takara Bio) or NEBuilder HiFi (New England Biolabs), replacing the FLEX-mCherry construct originally in the vector. Descriptions of all the constructs tested are listed in Supplementary Table 1. The constructs used for multiplexed EM labeling in the study are bolded in Supplementary Table 1. All constructs were verified using Sanger sequencing and maintained in NEB Stable *E. coli* (New England Biolabs). Plasmids generated in this study (Table 1) were deposited to Addgene.

Cell culture and transfection

HEK293T cells were maintained in DMEM (Thermo Fisher) supplemented with 10% FBS (Thermo Fisher), and split when confluency reached ~80% with trypsin/EDTA (Thermo Fisher). Transfections were carried out using polyethylenimine (PEI, linear, MW 25K, Polysciences) with PEI:DNA ratio of 4:1 at in PBS (pH 7.4) at ~50% confluency.

AAV production

AAV productions were carried out according to a previously described protocol[47]. Briefly, HEK293T cells were triply transfected with an AAV genome plasmid, a Rep/Cap plasmid of the desired serotype, and the pHelper plasmid using PEI. Cells were maintained for 5 days with media collection on day 3. Culture media were concentrated using polyethylene glycol (MW 8K, MilliporeSigma), and cells were digested using Salt Active Nuclease (ArcticZymes). The AAVs were further purified from the lysates using discontinuous

iodixanol (MilliporeSigma) gradients, and finally diafiltrated using Amicon Ultra (100K NMWL, Millipore) with PBS with 0.001% Pluronic F-68 (Thermo Fisher). AAV titers were determined using qPCR as DNase-I-resistant viral genomes (vg). Typical final concentrations obtained for AAV1 were $\sim 3 \times 10^{13}$ vg/mL, and for AAV9 were $\sim 3 \times 10^{14}$ vg/mL.

Viral injections

For all injections Fast Green FCF dye (MilliporeSigma) was included to aid visualization.

For IP AAV9 injections, $\sim 1 \times 10^{12}$ vg was delivered through glass pipettes into P0-P1 animals after the animals were anesthetized with ice.

For all parenchymal AAV1 injections, viruses were diluted to final concentrations of 3×10^{12}-1×10^{13} vg/mL each before injection. 3-4 injections were made on different sites and 50-100 nL was injected at each site. For non-stereotactic cortical AAV1 injections, P1-P3 animals were anesthetized with ice, and viruses were injected into the cortex using glass pipettes directly through the skulls. For stereotactic cortical AAV1 injections, P21 animals were anesthetized with isoflurane, and viruses were injected into S1 forelimb area using glass pipettes through drilled holes in the skull. For spinal cord AAV1 injections, P12-P14 animals were anesthetized with isoflurane, and viruses were injected into the cervical spinal cord using glass pipettes directly through the meninges.

Immunohistochemistry and confocal imaging

Mice were transcardially perfused with Ames' medium (MilliporeSigma) containing heparin (MilliporeSigma) (oxygenated with 95% O_2, 5% CO_2, warmed to 37 °C) to remove blood, and then 4% paraformaldehyde (Electron Microscopy Sciences) in 0.1 M PB (pH 7.4, warmed to 37 °C). Tissues were dissected out and then post-fixed in the same fixative at 4°C overnight. After washing with PBS, tissues were cryoprotected using PBS containing 30% sucrose (MilliporeSigma) at 4°C overnight. Tissues were then embedded in OCT (Sakura Finetek) and frozen with dry ice. 25 μm sections were prepared using a Leica CM3050 S cryostat, and dried on slides for 30 min. Sections were rehydrated with PBS for 3×5 min, and then blocked with PBS containing 5% Normal Goat Serum (Vector Labs) and 0.1% Triton X-100 (MilliporeSigma) ("blocking solution") for 1 hour. Sections were then stained with primary antibodies diluted in blocking solution at 4°C overnight. Sections were washed with PBS containing 0.02% Tween-20 (MilliporeSigma) for 4×5 min, and then stained with secondary antibodies diluted in blocking solution at 4°C overnight. Sections were then washed with PBS containing 0.02% Tween 20 for 4×5 min, and mounted with Fluoromount-G (SouthernBiotech). Slides were imaged with a Zeiss LSM 700 laser scanning confocal microscope as Z-stacks. Maximum intensity projections were made, and image intensities were adjusted using Fiji/ImageJ.

Primary antibodies used were rabbit anti-DsRed polyclonal (1:500, Takara Bio, 632496) and mouse anti-NeuN, clone A60 (1:1000, Millipore, MAB377). Secondary antibodies used were goat anti-Rabbit IgG (H+L) highly cross-adsorbed, Alexa 546 (1:500, Thermo Fisher, A-11035) and goat anti-Mouse IgG1 cross-adsorbed, Alexa 488 (1:500, Thermo Fisher, A-21121). All antibodies were validated by the manufacturers.

Mice

All mice used in the study are of mixed background.

$Th^{T2A-CreER}$ (JAX 025614)[31] was used to label C-LTMRs. $Mrgprd^{Cre}$[32] was used to label Mrgprd$^+$ afferents. $Mrgprb4^{Cre}$ (JAX 021077)[33] was used to label Mrgprb4$^+$ afferents. Tg(Rbp4-Cre)KL100 (MMRRC 037128)[27] was used to label layer 5 corticofugal neurons. $Slc32a1^{IRES-Cre}$ (JAX 028862)[38] was used to label all inhibitory neurons. $Pvalb^{T2A-FlpO}$ (JAX 022730)[36] was used to label fast-spiking GABAergic cortical interneurons. $Avil^{FlpO}$, which expresses FlpO recombinase in somatosensory neurons and will be described elsewhere, was used to label all somatosensory afferents. $Scn10a^{Cre}$[41] was used to label all Na$_V$1.8$^+$ neurons.

Animals were sacrificed 2-3 weeks after AAV injections or tamoxifen administration, whichever came later (median P21, range P21-P35).

Tamoxifen administration

Tamoxifen (MilliporeSigma) was dissolved in ethanol (MilliporeSigma) to 10 mg/mL and then mixed with an equal volume of sunflower seed oil (MilliporeSigma). The mixture was vortexed, and ethanol was then removed under vacuum. The final solution was delivered to animals via IP injection.

Generation of mouse lines

DNA fragments were amplified by PCR using Q5 Hot Start and cloned into the targeting vector used to create the Ai65 mouse line[36]. In-Fusion HD or NEBuilder HiFi was used to replace the tdTomato coding sequences of the Ai65 tageting vector (Addgene plasmid # 61577) to generate $ROSA26^{DR-Matrix-dAPEX2}$ and $ROSA26^{DR-ER-dAPEX2}$ targeting vectors. Targeting vectors were linearized using KpnI-HF (New England Biolabs), and 129S4/SvJae ES cells (J1) were transfected for homologous recombination and selected using neomycin. ES cells harboring successful integrations were screened using long-range PCR for both 5'- and 3'-arms. Properly recombined and karyotypically normal ES cells were then injected into blastocysts to generate chimeras. Germline transmission of the targeted alleles was established to obtain F1 animals. For generation of mouse lines harboring the single-recombinase-dependent alleles, dual-recombinase-dependent $ROSA26^{DR-Matrix-dAPEX2}$ and $ROSA26^{DR-ER-dAPEX2}$ mouse lines were crossed to the germline deleter lines EIIa-Cre (JAX 003724)[48] and Actb-Flpe (JAX 005703)[49] to excise the loxP-STOP-loxP and frt-STOP-frt cassettes, respectively. Mouse lines generated in this study (Table 2) were deposited to the Jackson Laboratory.

Determination of optimal staining conditions

Given the wide range of reaction conditions reported for peroxidase staining[11, 12, 14, 23, 50], we systematically determined the optimal condition for peroxidase staining with dAPEX2 expressed in mice. We tested a range of hydrogen peroxide concentrations (0.0003% to 0.03%) as well as DAB concentrations (0.1 mg/mL to 1 mg/mL) (Supplementary Fig. 3). We found that 0.003% hydrogen peroxide gave the highest staining intensity regardless of the DAB concentration. Staining intensity observed under LM is positively correlated with DAB

concentration, however we found that if the DAB concentration is too high staining artifacts could occur (Supplementary Fig. 4). Therefore, we determined 0.003% hydrogen peroxide and 0.3 mg/mL DAB to be the optimal concentrations for staining. We also found that including saponin during peroxidase staining[11] degraded ultrastructure (data not shown). Adding a sodium hydrosulfite reduction step as previously reported[14] did not lead to any perceivable difference in EM (data not shown), and we speculate that this might be due to our use of a lower hydrogen peroxide concentration in comparison, which presumably did not oxidize the samples as much.

We noticed that when the peroxidase labeling density is extremely high, such as in the cortex after injection of large amounts of constitutive AAV1 vectors, staining penetration issues could occur. It appeared that this was due to local reactant depletion since a more sparsely labeled region in the same slice stained in the same well (e.g. the thalamus) did not have this issue. This issue was not apparent when labeling density was lower as was typical in most experiments. We recommend using thinner vibratome sections (e.g. 100 μm) when staining penetration is a concern.

We also determined the optimal EM sample preparation protocol that best preserves DAB staining while providing sufficient counterstaining for synapse analysis. The osmium-only protocol (see below for details) led to clear DAB staining but minimal contrast in membrane and synaptic density (data not shown), while the rOTO protocol yielded excellent contrast, spurious DAB staining artifacts could be seen with the Matrix-dAPEX2 construct (Supplementary Fig. 5). The rOTO protocol (see below for details) did not cause any issue with the ER-dAPEX2 construct and was successfully used in a double labeling experiment equivalent to that in Fig. 3a (Supplementary Fig. 5c), suggesting that rOTO is compatible with this technique when distinguishing the two mitochondrial constructs is not needed and heavy metal impregnation is desired. Therefore, we used a reduced osmium protocol (see below for details) which afforded a balance between the ability to distinguish DAB staining and section counterstaining contrast (Supplementary Fig. 5).

Electron microscopy

Mice were transcardially perfused with Ames' medium containing heparin (oxygenated with 95% O_2, 5% CO_2, warmed to 37 °C) to remove blood, and then with a buffer containing 0.15 M sodium cacodylate (Electron Microscopy Sciences) (pH 7.4) and 0.04% $CaCl_2$ (MilliporeSigma) (cacodylate buffer) with 2.5% glutaraldehyde (Electron Microscopy Sciences) and 2% paraformaldehyde (warmed to 37 °C). Tissues were dissected out and then post-fixed in the same fixative at 4°C overnight. Skin samples were first shaved and then the adipose layer beneath the dermis was removed. After washing tissues with cacodylate buffer, tissues were embedded in low-melting-point agarose (Thermo Fisher), and 100-200 μm sections were taken in cacodylate buffer using a Leica VT1000 S vibratome. Sections were washed 2×10 min with cacodylate buffer containing 50 mM glycine (MilliporeSigma), 1×10 min with cacodylate buffer, and then incubated in 1 mL of 3,3'-diaminobenzidine tetrahydrochloride hydrate (MilliporeSigma) (DAB; 0.3 mg/mL) in cacodylate buffer in the dark for 30 min. 10 μL of cacodylate buffer containing 0.3% H_2O_2 (MilliporeSigma) was then added to the DAB solution directly (final H_2O_2 concentration: 0.003%) to initiate the

peroxidase reaction. The reaction was allowed to proceed in the dark for 1 hour, and sections were then washed with cacodylate buffer. Stained sections were then fixed with cacodylate buffer containing 3% glutaraldehyde at 4°C overnight. Sections were washed with cacodylate buffer, followed by cacodylate buffer containing 50 mM glycine, and then cacodylate buffer. For reduced osmium staining (used for all figures unless otherwise noted), sections were osmicated in cacodylate buffer containing 1% osmium tetroxide (Electron Microscopy Sciences)/1.5% potassium ferrocyanide (MilliporeSigma) for 1 hour. Sections were then washed with ddH_2O, and stained in a solution containing 0.05 M sodium maleate (MilliporeSigma) (pH 5.15) and 1% uranyl acetate (Electron Microscopy Sciences) at 4°C overnight. After washing with ddH_2O, sections were dehydrated with an ethanol series followed by propylene oxide (Electron Microscopy Sciences). Sections were then infiltrated with 1:1 epoxy resin mix (LX-112, Ladd Research):propylene oxide at 4°C overnight. Finally, sections were embedded in epoxy resin mix and cured at 60°C for 48-72 hours.

For osmium-only staining, sections were processed as described above up to but not including the osmication step, and then osmicated with an aqueous solution containing 1% osmium tetroxide for 30 min, and washed with ddH_2O. Dehydration and embedding were done as described above.

For reduced-osmium-thiocarbohydrazide-osmium (rOTO) staining, sections were stained following a slightly modified previously reported protocol[51]. Sections were processed as described above up to but not including the osmication step, and osmicated with cacodylate buffer containing 2% osmium tetroxide for 1 hour, and reduced in cacodylate buffer containing 2.5% potassium ferrocyanide for 1 hour, and then washed with ddH_2O. Then sections were incubated in a filtered aqueous solution containing 1% thiocarbohydrazide (Electron Microscopy Sciences) at 40°C for 15 min, and washed with ddH_2O. Sections were osmicated again with an aqueous solution containing 2% osmium tetroxide for 1 hour, and washed with ddH_2O. Then sections were incubated in a solution containing 0.05 M sodium maleate (pH 5.15) and 1% uranyl acetate overnight at 4°C. Sections were warmed to 50°C for 2 hours in the uranyl acetate solution and then washed with ddH_2O. Dehydration and embedding proceeded as described above.

For HEK293T cells, cells were fixed with cacodylate buffer containing 2.5% glutaraldehyde and 2% paraformaldehyde for 30 min, and washed with cacodylate buffer containing 50 mM glycine followed by cacodylate buffer. Peroxidase reactions were initiated with cacodylate buffer containing 0.003% H_2O_2 and 0.3 mg/mL DAB, and allowed to proceed for 15 min. Cells were then washed with cacodylate buffer and scraped off the plate. Scraped cells were then prepared for EM with the osmium-only staining protocol described above.

Samples were sectioned using a Leica EM UC7 ultramicrotome with Diatome diamond knives, and ultrathin sections (40 nm) were picked up on glow-discharged formvar/carbon films on slot grids (Ted Pella). For single sections, ultrathin sections were imaged using a JEOL 1200EX transmission electron microscope at 80 kV accelerating voltage and 10,000x nominal magnification with an AMT XR-611 CCD camera at a final pixel size of 1.84 nm. Micrographs were excluded from analysis if they were out-of-focus, had inappropriate

background correction, or had debris or other artifacts obscuring the field of view. Images were adjusted with normalization using Fiji/ImageJ to enhance contrast.

For serial sections, 50 ultrathin sections were manually picked up and imaged using a JEOL 1200EX transmission electron microscope at 120 kV accelerating voltage and 2,500x nominal magnification with an XIMEA CB200MG-CM CMOS camera at a final pixel size of 4.26 nm. Sections 45-47 were lost during imaging. Images were adjusted with contrast limited adaptive histogram equalization using Fiji/ImageJ to reduce intensity variation across different imaging fields. Individual images were then elastically montaged and aligned using TrakEM2[52–54]. Neuronal profiles, mitochondria and synapses were manually reconstructed using TrakEM2. For 3D visualization, arealists were interpolated using TrakEM2, and meshes were smoothed using ImageJ 3D Viewer to generate 3D models with smooth surfaces.

For quantification of discriminability of Matrix-dAPEX2 vs. IMS-dAPEX2, two annotators (Q.Z. and D.L.P.) independently categorized all the mitochondria in the volume as either matrix-labeled, IMS-labeled, or unlabeled based on the features of the staining derived from single labeling experiments. Then the level of concordance was assessed by comparing the annotations, with the possible outcomes as matching matrix-labeled annotation, matching IMS-labeled annotation, matching unlabeled annotation, mismatching matrix-labeled vs. IMS-labeled annotation, mismatching matrix-labeled vs. unlabeled annotation, and mismatching IMS-labeled vs. unlabeled annotation. Objects on either surface of the volume were not quantified if they only spanned 3 or fewer sections. 12 objects were excluded from the analysis because at least one annotator could not ascertain whether they were mitochondria or not (for 10 of these 12 objects neither annotator could ascertain the identity of the object), because of the small size, obscuration by artifacts, or lack of internal ultrastructure.

Bright-field light microscopy

Sections were processed as described above for electron microscopy up to but not including the osmication step. Then sections were dehydrated with a methanol (MilliporeSigma) series and cleared with 1:2 benzyl alcohol (MilliporeSigma)/benzyl benzoate (MilliporeSigma) (BABB). Cleared sections were mounted with BABB and imaged with an Olympus BX63 using 4x, 10x or 20x objectives. White balance was individually calibrated for each slide, and lighting and exposure times were controlled for all comparison groups.

Reporting Summary

Further information on experimental design is available in the Nature Research Reporting Summary linked to this article.

Data Availability Statement

The authors declare that the data supporting the findings of this study are available within the paper and its supplementary information files.

Supplementary Material

Refer to Web version on PubMed Central for supplementary material.

Acknowledgements

References

1. Daigle TL, et al. A Suite of Transgenic Driver and Reporter Mouse Lines with Enhanced Brain-Cell-Type Targeting and Functionality. Cell 174, 465–480 e422 (2018). [PubMed: 30007418]

2. Zhu F, et al. Architecture of the Mouse Brain Synaptome. Neuron 99, 781–799 e710 (2018). [PubMed: 30078578]

3. Feinberg EH, et al. GFP Reconstitution Across Synaptic Partners (GRASP) defines cell contacts and synapses in living nervous systems. Neuron 57, 353–363 (2008). [PubMed: 18255029]

4. Martell JD, et al. A split horseradish peroxidase for the detection of intercellular protein-protein interactions and sensitive visualization of synapses. Nat. Biotechnol 34, 774–780 (2016). [PubMed: 27240195]

5. Dani A, Huang B, Bergan J, Dulac C & Zhuang X Superresolution imaging of chemical synapses in the brain. Neuron 68, 843–856 (2010). [PubMed: 21144999]

6. Karagiannis ED & Boyden ES Expansion microscopy: development and neuroscience applications. Curr. Opin. Neurobiol 50, 56–63 (2018). [PubMed: 29316506]

7. Morgan JL, Berger DR, Wetzel AW & Lichtman JW The Fuzzy Logic of Network Connectivity in Mouse Visual Thalamus. Cell 165, 192–206 (2016). [PubMed: 27015312]

8. Zheng Z, et al. A Complete Electron Microscopy Volume of the Brain of Adult Drosophila melanogaster. Cell 174, 730–743 e722 (2018). [PubMed: 30033368]

9. Hildebrand DGC, et al. Whole-brain serial-section electron microscopy in larval zebrafish. Nature 545, 345–349 (2017). [PubMed: 28489821]

10. Kasthuri N, et al. Saturated Reconstruction of a Volume of Neocortex. Cell 162, 648–661 (2015). [PubMed: 26232230]

11. Atasoy D, et al. A genetically specified connectomics approach applied to long-range feeding regulatory circuits. Nat. Neurosci 17, 1830–1839 (2014). [PubMed: 25362474]

12. Li J, Wang Y, Chiu SL & Cline HT Membrane targeted horseradish peroxidase as a marker for correlative fluorescence and electron microscopy studies. Front. Neural Circuits 4, 6 (2010). [PubMed: 20204144]

13. Schikorski T, Young SM Jr. & Hu Y Horseradish peroxidase cDNA as a marker for electron microscopy in neurons. J. Neurosci. Methods 165, 210–215 (2007). [PubMed: 17631969]

14. Joesch M, et al. Reconstruction of genetically identified neurons imaged by serial-section electron microscopy. Elife 5 (2016).

15. Leal-Ortiz S, et al. Piccolo modulation of Synapsin1a dynamics regulates synaptic vesicle exocytosis. J Cell Biol. 181, 831–846 (2008). [PubMed: 18519737]

16. Shu X, et al. A genetically encoded tag for correlated light and electron microscopy of intact cells, tissues, and organisms. PLoS Biol. 9, e1001041 (2011). [PubMed: 21483721]

17. Adams SR, et al. Multicolor Electron Microscopy for Simultaneous Visualization of Multiple Molecular Species. Cell Chem. Biol 23, 1417–1427 (2016). [PubMed: 27818300]

Author Manuscript

Author Manuscript

Author Manuscript

Author Manuscript

18. Drawitsch F, Karimi A, Boergens KM & Helmstaedter M Fluo EM, virtual labeling of axons in three-dimensional electron microscopy data for long-range connectomics. Elife 7 (2018).

19. Fang T, et al. Nanobody immunostaining for correlated light and electron microscopy with preservation of ultrastructure. Nat. Methods 15, 1029–1032 (2018). [PubMed: 30397326]

20. Lin TY, et al. Mapping chromatic pathways in the Drosophila visual system. J. Comp. Neurol 524, 213–227 (2016). [PubMed: 26179639]

21. Machida A, et al. Intraperitoneal administration of AAV9-shRNA inhibits target gene expression in the dorsal root ganglia of neonatal mice. Mol. Pain 9, 36 (2013). [PubMed: 23866078]

22. Rhee HW, et al. Proteomic mapping of mitochondria in living cells via spatially restricted enzymatic tagging. Science 339, 1328–1331 (2013). [PubMed: 23371551]

23. Han C, et al. Integrins regulate repulsion-mediated dendritic patterning of drosophila sensory neurons by restricting dendrites in a 2D space. Neuron 73, 64–78 (2012). [PubMed: 22243747]

24. Lam SS, et al. Directed evolution of APEX2 for electron microscopy and proximity labeling. Nat. Methods 12, 51–54 (2015). [PubMed: 25419960]

25. Hung V, et al. Spatially resolved proteomic mapping in living cells with the engineered peroxidase APEX2. Nat. Protoc 11, 456–475 (2016). [PubMed: 26866790]

26. Martell JD, et al. Engineered ascorbate peroxidase as a genetically encoded reporter for electron microscopy. Nat. Biotechnol 30, 1143–1148 (2012). [PubMed: 23086203]

27. Gerfen CR, Paletzki R & Heintz N GENSAT BAC cre-recombinase driver lines to study the functional organization of cerebral cortical and basal ganglia circuits. Neuron 80, 1368–1383 (2013). [PubMed: 24360541]

28. Abraira VE & Ginty DD The sensory neurons of touch. Neuron 79, 618–639 (2013). [PubMed: 23972592]

29. Sugiura Y, Lee CL & Perl ER Central projections of identified, unmyelinated (C) afferent fibers innervating mammalian skin. Science 234, 358–361 (1986). [PubMed: 3764416]

30. Alvarez FJ, Kavookjian AM & Light AR Ultrastructural morphology, synaptic relationships, and CGRP immunoreactivity of physiologically identified C-fiber terminals in the monkey spinal cord. J. Comp. Neurol 329, 472–490 (1993). [PubMed: 7681070]

31. Abraira VE, et al. The Cellular and Synaptic Architecture of the Mechanosensory Dorsal Horn. Cell 168, 295–310 e219 (2017). [PubMed: 28041852]

32. Rau KK, et al. Mrgprd enhances excitability in specific populations of cutaneous murine polymodal nociceptors. J. Neurosci 29, 8612–8619 (2009). [PubMed: 19571152]

33. Vrontou S, Wong AM, Rau KK, Koerber HR & Anderson DJ Genetic identification of C fibres that detect massage-like stroking of hairy skin in vivo. Nature 493, 669–673 (2013). [PubMed: 23364746]

34. Ribeiro-da-Silva A & Coimbra A Two types of synaptic glomeruli and their distribution in laminae I-III of the rat spinal cord. J. Comp. Neurol 209, 176–186 (1982). [PubMed: 6890076]

35. Castle MJ, Turunen HT, Vandenberghe LH & Wolfe JH Controlling AAV Tropism in the Nervous System with Natural and Engineered Capsids. Methods Mol. Biol 1382, 133–149 (2016). [PubMed: 26611584]

36. Madisen L, et al. Transgenic mice for intersectional targeting of neural sensors and effectors with high specificity and performance. Neuron 85, 942–958 (2015). [PubMed: 25741722]

37. Hu H, Gan J & Jonas P Interneurons. Fast-spiking, parvalbumin(+) GABAergic interneurons: from cellular design to microcircuit function. Science 345, 1255263 (2014). [PubMed: 25082707]

38. Vong L, et al. Leptin action on GABAergic neurons prevents obesity and reduces inhibitory tone to POMC neurons. Neuron 71, 142–154 (2011). [PubMed: 21745644]

39. Rudomin P & Schmidt RF Presynaptic inhibition in the vertebrate spinal cord revisited. Exp. Brain. Res 129, 1–37 (1999). [PubMed: 10550500]

40. Valtschanoff JG, Weinberg RJ & Rustioni A Amino acid immunoreactivity in corticospinal terminals. Exp. Brain. Res 93, 95–103 (1993). [PubMed: 7682185]

41. Nassar MA, et al. Nociceptor-specific gene deletion reveals a major role for Nav1.7 (PN1) in acute and inflammatory pain. Proc. Natl. Acad. Sci. U. S. A 101, 12706–12711 (2004). [PubMed: 15314237]

42. Shields SD, et al. Nav1.8 expression is not restricted to nociceptors in mouse peripheral nervous system. Pain 153, 2017–2030 (2012). [PubMed: 22703890]

43. Ng J, et al. Genetically targeted 3D visualisation of Drosophila neurons under Electron Microscopy and X-Ray Microscopy using miniSOG. Sci. Rep 6, 38863 (2016). [PubMed: 27958322]

44. Bock DD, et al. Network anatomy and in vivo physiology of visual cortical neurons. Nature 471, 177–182 (2011). [PubMed: 21390124]

45. Lee WC, et al. Anatomy and function of an excitatory network in the visual cortex. Nature 532, 370–374 (2016). [PubMed: 27018655]

46. Briggman KL, Helmstaedter M & Denk W Wiring specificity in the direction-selectivity circuit of the retina. Nature 471, 183–188 (2011). [PubMed: 21390125]

Method-only References

47. Deverman BE, et al. Cre-dependent selection yields AAV variants for widespread gene transfer to the adult brain. Nat. Biotechnol 34, 204–209 (2016). [PubMed: 26829320]

48. Lakso M, et al. Efficient in vivo manipulation of mouse genomic sequences at the zygote stage. Proc. Natl. Acad. Sci. U. S. A 93, 5860–5865 (1996). [PubMed: 8650183]

49. Rodriguez CI, et al. High-efficiency deleter mice show that FLPe is an alternative to Cre-loxP. Nat. Genet 25, 139–140 (2000). [PubMed: 10835623]

50. Martell JD, Deerinck TJ, Lam SS, Ellisman MH & Ting AY Electron microscopy using the genetically encoded APEX2 tag in cultured mammalian cells. Nat. Protoc 12, 1792–1816 (2017). [PubMed: 28796234]

51. Hua Y, Laserstein P & Helmstaedter M Large-volume en-bloc staining for electron microscopy-based connectomics. Nat. Commun 6, 7923 (2015). [PubMed: 26235643]

52. Cardona A, et al. TrakEM2 software for neural circuit reconstruction. PLoS One 7, e38011 (2012). [PubMed: 22723842]

53. Saalfeld S, Cardona A, Hartenstein V & Tomancak P As-rigid-as-possible mosaicking and serial section registration of large ssTEM datasets. Bioinformatics 26, i57–63 (2010). [PubMed: 20529937]

54. Saalfeld S, Fetter R, Cardona A & Tomancak P Elastic volume reconstruction from series of ultra-thin microscopy sections. Nat. Methods 9, 717–720 (2012). [PubMed: 22688414]
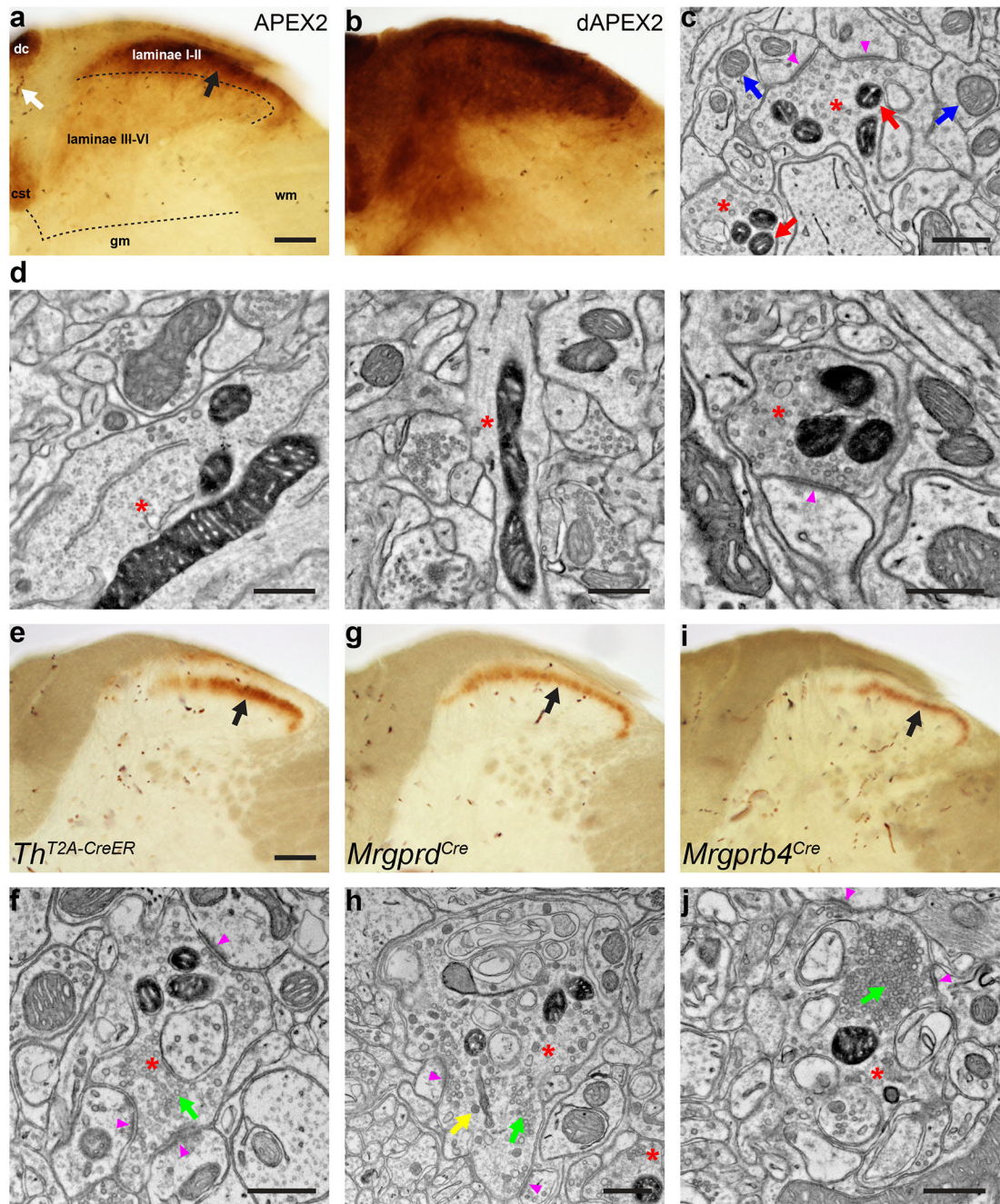
Figure 1. dAPEX2 is a sensitive reporter for visualizing axons of long projection neurons with EM

(**a**) LM image of the spinal cord dorsal horn after systemic transduction of AAV9-mito-V5-APEX2. Black arrow: staining from mito-V5-APEX2. Laminae I-II has much stronger staining than laminae III-VI. White arrow: endogenous peroxidase activity from erythrocytes. dc: dorsal column, cst: corticospinal tract, gm: grey matter, wm: white matter. n = 4 animals and experiments.

(**b**) LM image of the spinal cord dorsal horn after systemic transduction of AAV9-Matrix-dAPEX2. Note the robust staining in laminae III-VI with Matrix-dAPEX2 and generally increased staining levels compared to mito-V5-APEX2. n = 6 animals and experiments.

(**c**) EM image of the spinal cord dorsal horn after systemic transduction of AAV9-Matrix-dAPEX2. Asterisks: labeled axon terminals. Red arrows: labeled mitochondria. Blue arrows: unlabeled mitochondria. Arrowheads: synapses made by the labeled axon terminals. Note that ultrastructural details of the labeled neurons are not obscured by staining products. n = 3 animals and experiments.

(**d**) EM images of a cortical layer 5 neuron labeled using Tg(Rbp4-Cre)KL100 and AAV1-DIO-Matrix-dAPEX2 (asterisks). (Left) Soma of a labeled neuron. (Middle) Dendrite of a labeled neuron. (Right) Corticospinal axon in the spinal cord dorsal horn of a cortical layer 5 neuron labeled using Tg(Rbp4-Cre)KL100. Arrowhead: synapse made by the labeled neuron. n = 2 animals and experiments.

(**e**) LM image of spinal cord dorsal horn from a $Th^{T2A-CreER}$ animal transduced with AAV9-DIO-Matrix-dAPEX2 and treated with tamoxifen from P14-21 to label C-LTMRs. Arrow: staining from labeled C-LTMR axons. n = 6 animals and experiments.

(**f**) EM image from the same animal in **e**. Asterisk: labeled C-LTMR axon terminal with round, clear vesicles (green arrow). Most C-LTMR axon terminals have only clear vesicles. Arrowheads: synapses made by the labeled C-LTMR terminal. n = 4 animals and experiments.

(**g**) LM image of spinal cord dorsal horn from an $Mgprd^{Cre}$ animal transduced with AAV9-DIO-Matrix-dAPEX2. Arrow: staining from labeled Mrgprd$^+$ polymodal nociceptor afferents. n = 4 animals and experiments.

(**h**) EM image from the same animal in **g**. Asterisk: labeled Mrgprd$^+$ polymodal nociceptor axon terminal. Unlike C-LTMRs, these neurons can exhibit both round, clear vesicles (green arrow) and large, variably shaped dense-core vesicles (yellow arrow). Arrowheads: synapses made by the labeled Mrgprd$^+$ polymodal nociceptor axon terminal. n = 3 animals and experiments.

(**i**) LM image of spinal cord dorsal horn from an $Mrgprb4^{Cre}$ animal transduced with AAV9-DIO-Matrix-dAPEX2. Arrow: staining from labeled Mrgprb4$^+$ afferents. n = 4 animals and experiments.

(**j**) EM image from the same animal in **i**. Asterisk: labeled Mrgprb4$^+$ afferent axon terminal with a dense cluster of vesicles (green arrow), a configuration rarely seen in C-LTMRs, but often present in both Mrgprb4$^+$ and Mrgprd$^+$ afferents. Arrowheads: synapses made by the labeled Mrgprb4$^+$ afferent axon terminal. n = 3 animals and experiments.

Scale bars: **a, b**: 100 μm, **c, d**: 0.5 μm, **e, g, i**: 100 μm, **f, h, j**: 0.5 μm.

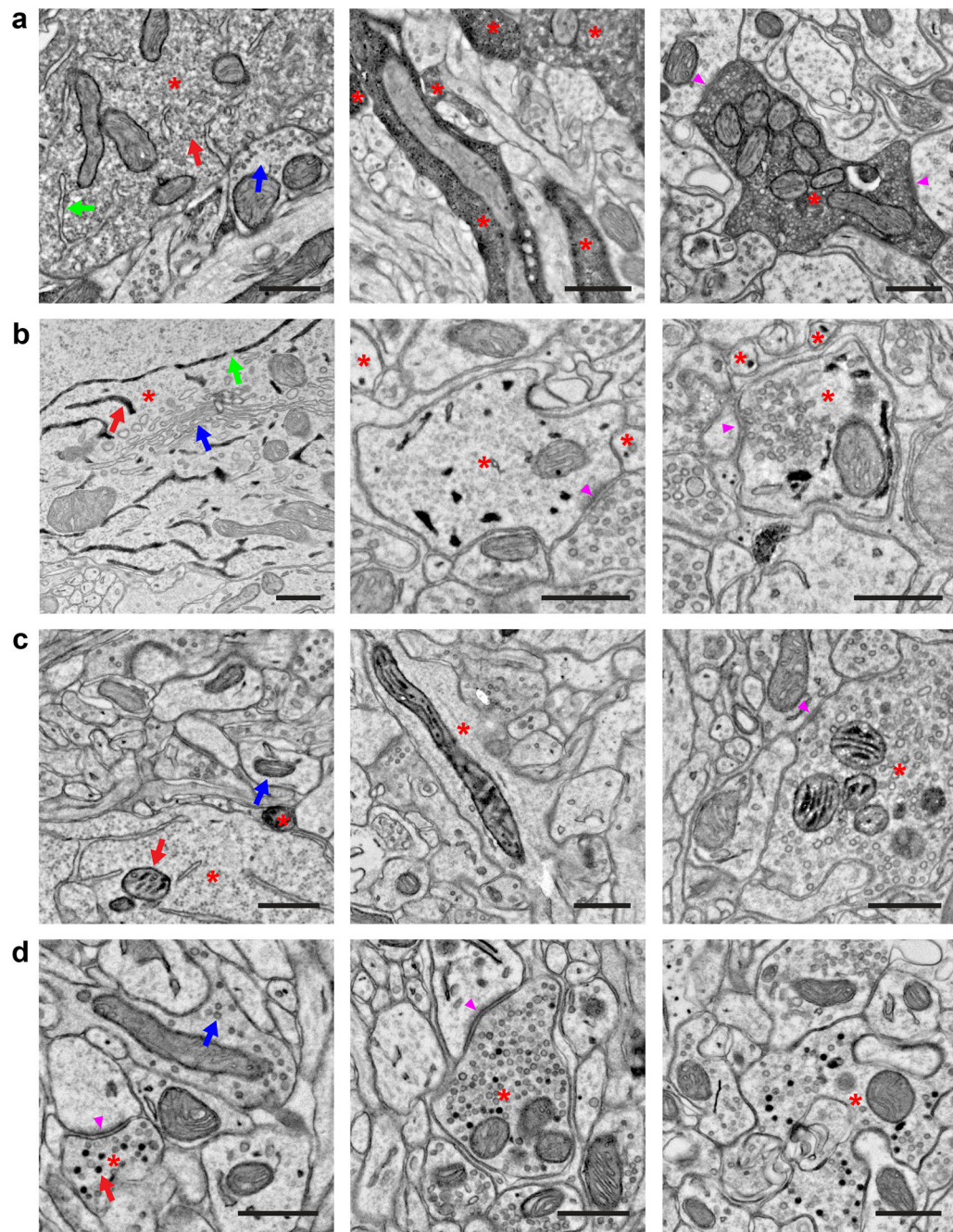**Figure 2. Peroxidase constructs targeted to different subcellular compartments for multiplexed EM labeling**

(**a**) EM images showing localization of dAPEX2. Asterisks: labeled neurons. Staining in the cytoplasm is often not uniform and can appear granular. (Left) Soma of a cortical layer 5 neuron labeled using Tg(Rbp4-Cre)KL100. Red arrow: labeled cytoplasm. Blue arrow: unlabeled cytoplasm. Note that membrane-limited organelles, such as ER (green arrow), mitochondria, and Golgi apparatus, can usually be distinguished in stained cells. (Middle) Dendrites of cortical layer 5 neurons labeled using Tg(Rbp4-Cre)KL100. (Right) Axon of a primary sensory neuron in the spinal cord dorsal horn after AAV9 systemic transduction.

Arrowheads: synapses made by the labeled neuron. n = 2 animals and experiments for each condition.

(**b**) EM images showing localization of ER-dAPEX2. Asterisks: labeled neurons. (Left) Soma of a cortical layer 5 neuron labeled using Tg(Rbp4-Cre)KL100. Red arrow: labeled ER. Blue arrow: unlabeled Golgi apparatus. Note that nuclear envelope is labeled as expected and nuclear pores (green arrows) are clearly visible, unobscured by the reaction product. (Middle) Inhibitory interneurons in the dorsal horn labeled using $Slc32a1^{IRES\text{-}Cre}$. Arrowhead: a synapse received by an inhibitory interneuron. (Right) Inhibitory interneurons in the spinal cord dorsal horn labeled using $Slc32a1^{IRES\text{-}Cre}$. Arrowhead: a synapse made by an inhibitory interneuron. Note that identification of small ER profiles can be difficult and only clearly identified profiles are marked. n = 2 animals and experiments for each condition.

(**c**) EM images showing localization of IMS-dAPEX2. Asterisks: labeled neurons. (Left) Soma of a cortical layer 5 neuron labeled using Tg(Rbp4-Cre)KL100. Red arrow: labeled mitochondrion. Blue arrow: unlabeled mitochondrion. Preservation of the full extent of IMS staining is not always achieved, potentially due to difficulty in sectioning dense heavy metal labeling, however this usually does not hinder identification of stained mitochondria. (Middle) Dendrite of cortical layer 5 neuron labeled using Tg(Rbp4-Cre)KL100. (Right) Axon in the spinal cord dorsal horn after AAV9 systemic transduction. Arrowhead: synapse made by the labeled neuron. n = 2 animals and experiments for each condition.

(**d**) EM images showing localization of SV-HRP. Asterisks: labeled neurons. Not every vesicle in transduced cells is stained. (Left) Corticocortical axon of a cortical layer 5 neuron labeled using Tg(Rbp4-Cre)KL100. Red arrow: labeled vesicle. Blue arrow: unlabeled vesicle. Arrowhead: synapse made by the labeled neuron. (Middle) Corticospinal axon in the spinal cord dorsal horn of a cortical layer 5 neuron labeled using Tg(Rbp4-Cre)KL100. Arrowhead: synapse made by the labeled neuron. (Right) Axon in the spinal cord dorsal horn after AAV9 systemic transduction. n = 2 animals and experiments for each condition. Scale bars: 0.5 μm.
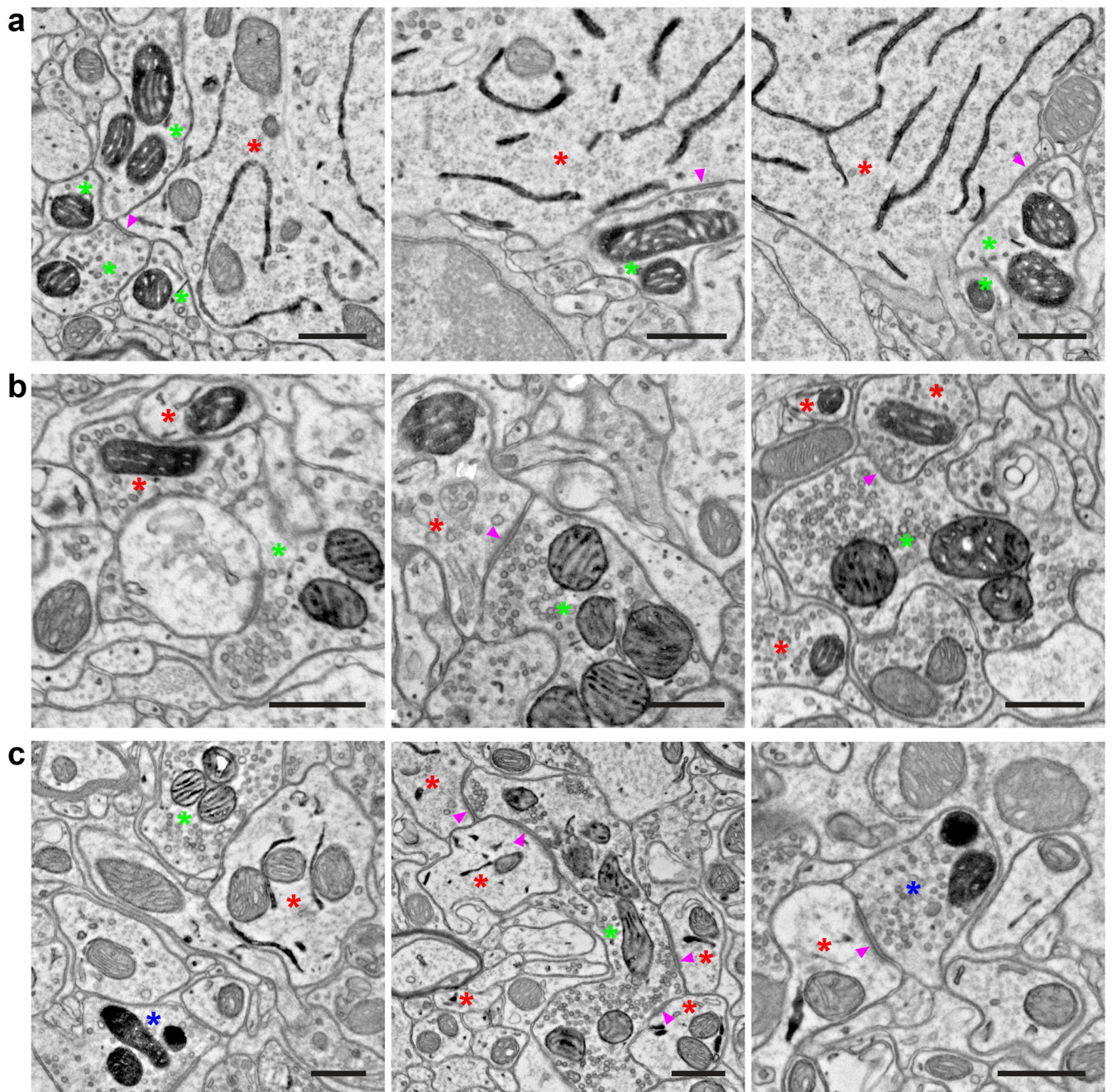
Figure 3. Double and triple EM labeling using orthogonal peroxidase reporter constructs
(**a**) EM images showing double labeling of cortical layer 5 pyramidal neurons (ER) using
Tg(Rbp4-Cre)KL100 and AAV1-DIO-ER-dAPEX2 (red asterisks), and fast-spiking
GABAergic interneurons (mitochondrial matrix) using $Pvalb^{T2A-FlpO}$ and AAV1-FDIO-
Matrix-dAPEX2 (green asterisks). Note the symmetric perisomatic synapses made by fast-
spiking interneurons onto layer 5 pyramidal neurons (arrowheads). n = 4 animals and
experiments.

(**b**) EM images showing double labeling of spinal cord dorsal horn inhibitory interneurons (mitochondrial matrix) using *Slc32a1*$^{IRES\text{-}Cre}$ and AAV1-DIO-Matrix-dAPEX2 (red asterisks), and primary somatosensory afferents (mitochondrial IMS) using *Avil*^{FlpO} and AAV9-FDIO-IMS-dAPEX2 (green asterisks). Arrowheads: an axodendritic synapse from a primary somatosensory afferent to an inhibitory interneuron (Middle) and an axoaxonic synapse from an inhibitory interneuron to a primary somatosensory afferent (Right). n = 3 animals and experiments.

(**c**) EM images showing triple labeling of dorsal horn inhibitory interneurons (ER) using *Slc32a1*$^{IRES\text{-}Cre}$ and AAV1-DIO-ER-dAPEX2 (red asterisks), primary somatosensory afferents (mitochondrial IMS) using *Avil*^{FlpO} and AAV9-FDIO-IMS-dAPEX2 (green asterisks), and corticospinal inputs (mitochondrial matrix) using cortical injections of AAV1-Matrix-dAPEX2 (blue asterisks). (Left) All three stains can be clearly visualized and distinguished in the same field of view. (Middle) A primary somatosensory afferent making axodendritic synaptic contacts onto inhibitory interneurons (arrowheads). Note the numerous synaptic contacts made by the primary somatosensory afferent, which is characteristic of the central axons of glomeruli. (Right) A corticospinal axon making an axodendritic synapse onto an inhibitory interneuron (arrowhead). This type of simple synaptic arrangement is typical of corticospinal inputs. n = 2 animals and experiments.
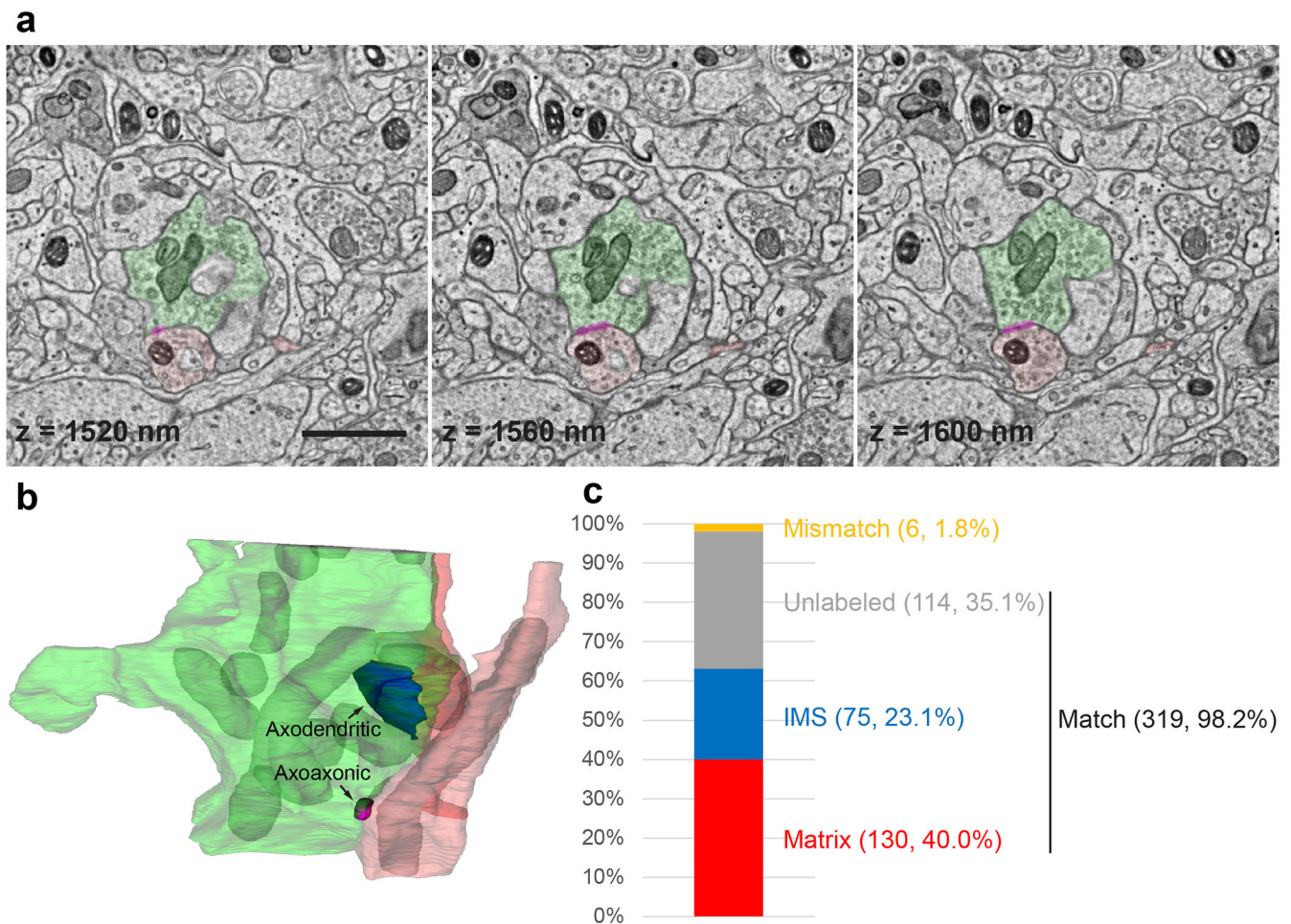
Scale bars: 0.5 μm.

Figure 4. Multiplexed peroxidase labeling in volume EM

(**a**) Three consecutive sections from one of the samples shown in Fig. 3b in which spinal cord dorsal horn inhibitory interneurons (mitochondrial matrix) were labeled using *Slc32a1*^{IRES-Cre} and AAV1-DIO-Matrix-dAPEX2 (axon in light red and dendrite in dark red), and primary somatosensory afferents (mitochondrial IMS) were labeled using *Avil*^{FlpO} and AAV9-FDIO-IMS-dAPEX2 (green). Magenta overlay: axoaxonic synapse between an inhibitory interneuron and the primary afferent. The z coordinates from the top of the volume are noted on each image. Scale bar: 1 μm. See also Supplementary Video 1.

(**b**) The 3D reconstruction of the same primary afferent and inhibitory interneuron profiles. Labeled mitochondria (grey) and an axodendritic synapse between the primary afferent and an inhibitory interneuron (blue) are additionally reconstructed. See also Supplementary Video 2.

(**c**) Level of concordance between independent annotations of mitochondria (matrix-labeled, IMS-labeled, or unlabeled) in a volume of $12 \times 8 \times 2$ μm by two annotators. The numbers of each category as well as their proportions of the total number of mitochondria are indicated in parentheses. The three categories Matrix, IMS, and Unlabeled all contain matching annotations, while the Mismatch category contains mismatching annotations.
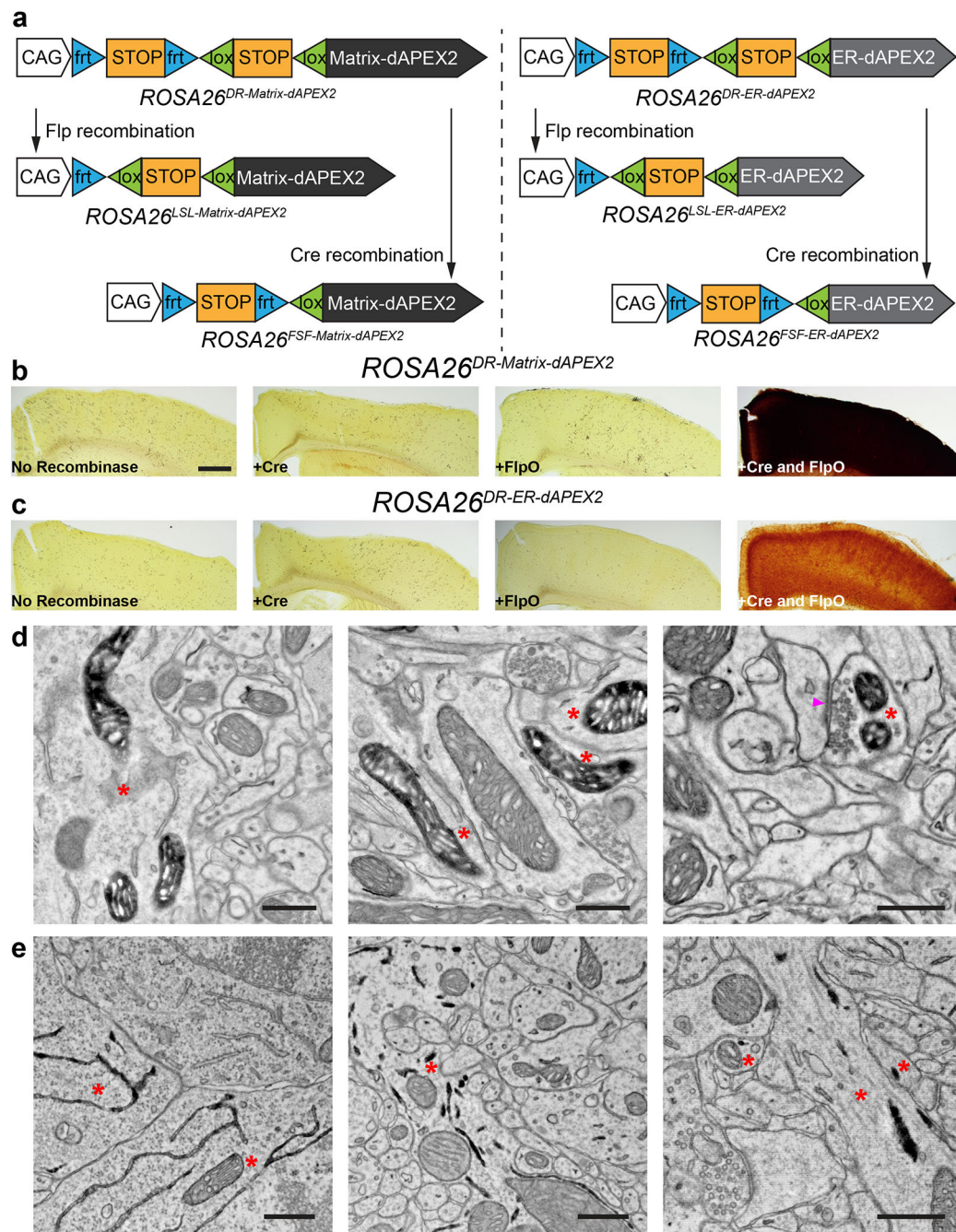
Figure 5. Generation of recombinase-dependent mouse dAPEX2 reporter lines

(**a**) Schematics showing overviews of the six mouse reporter lines. Single-recombinase-dependent lines were generated by germline deletion of one of the STOP cassettes.

(**b, c**) LM images showing cortical sections after injections of AAVs encoding various recombinases into dual-recombinase-dependent *ROSA26*[^DR-Matrix-dAPEX2] (**b**) and *ROSA26*[^DR-ER-dAPEX2] animals (**c**). Only endogenous peroxidase activity was observed when no recombinase, Cre alone, or FlpO alone was transduced (left three panels). dAPEX2

peroxidase staining was observed only following co-injection of Cre and FlpO viruses (rightmost panels).

(**d**) EM images from the cortex of a $ROSA26^{DR\text{-}Matrix\text{-}dAPEX2}$ animal co-transduced with Cre and FlpO. Asterisks: labeled neurons. Labeled mitochondria can be seen in soma, dendrites, and axons, consistent with results using AAVs to express peroxidase constructs. Arrowhead: synapse made by the labeled neuron. n = 4 animals and experiments.

(**e**) EM images of the cortex of a $ROSA26^{DR\text{-}ER\text{-}dAPEX2}$ animal co-transduced with Cre and FlpO. Asterisks: labeled neurons. Labeled ER can be seen in somata and dendrites, as expected. n = 4 animals and experiments.
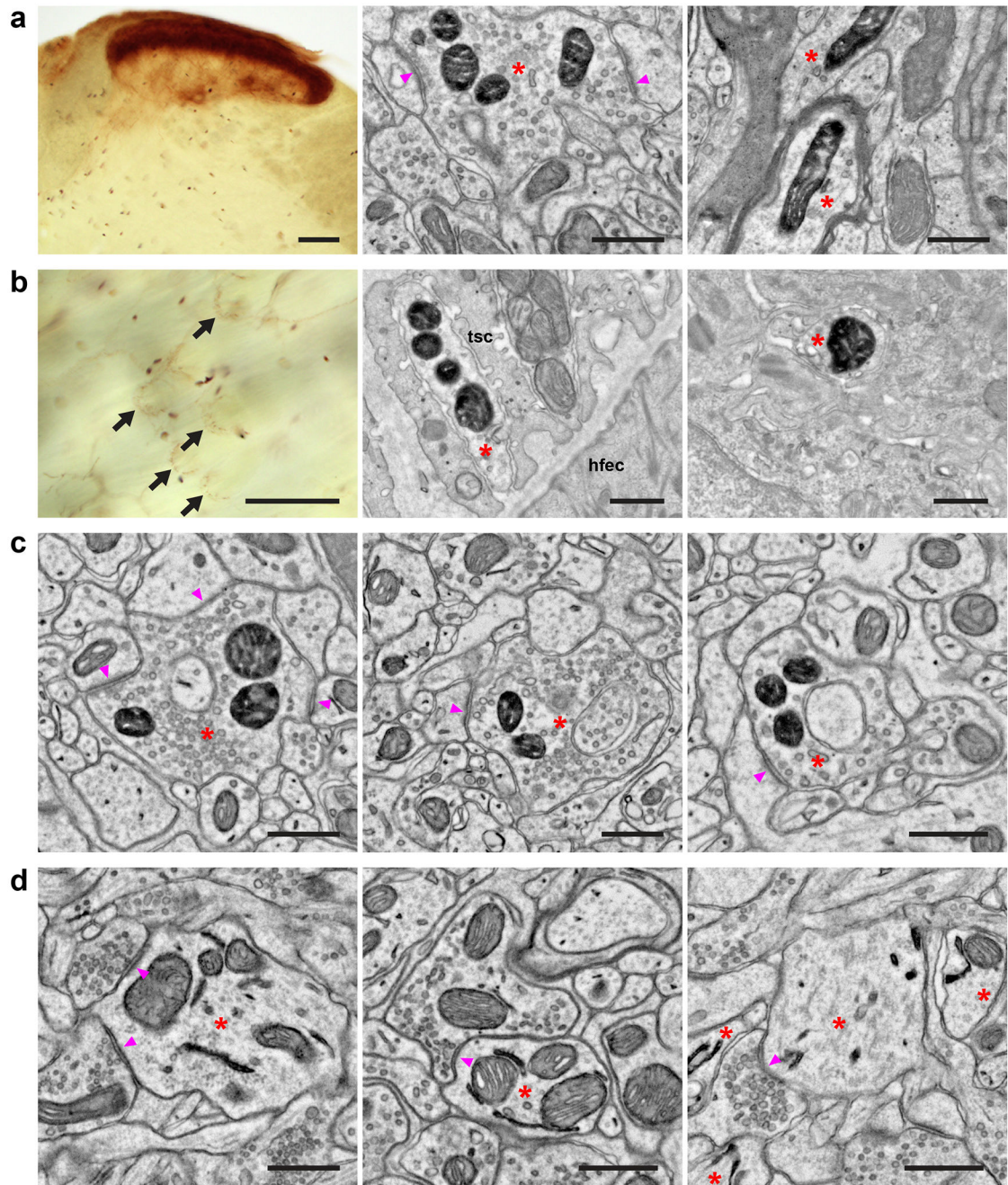
Scale bars: **b, c**: 500 μm, **d, e**: 0.5 μm.

Figure 6. Mouse dAPEX2 reporter lines exhibit robust EM staining
(**a**) Spinal cord dorsal horn images from an $Scn10a^{Cre}$; $Avil^{FlpO}$; $ROSA26^{DR-Matrix-dAPEX2}$ animal. (Left) LM image showing the expected pattern of heavy labeling in superficial laminae and lighter labeling in deep laminae expected from the expression of $Na_V1.8$ in both small- and a subset of large-diameter neurons. (Middle) EM image showing labeling in superficial laminae. Asterisk: labeled C-fiber axon terminal. Arrowheads: synapses made by the labeled C-fiber. (Right) EM image showing labeling in deep laminae. Asterisks: labeled axons. Note the myelination around one of the profiles. n = 2 animals and experiments.

(**b**) Skin images from an *Scn10a^{Cre}*; *Avil^{FlpO}*; *ROSA26$^{DR-Matrix-dAPEX2}$* animal. (Left) LM image showing labeled lanceolate endings (arrows). Free nerve endings are also labeled but not visible in this focal plane. (Middle) EM image showing a labeled lanceolate ending (asterisk) around a hair follicle. tsc: terminal Schwann cell, hfec: hair follicle epithelial cell. (Right) EM image showing a labeled free nerve ending (asterisk) in the epidermis. n = 2 animals and experiments.

(**c**) EM images from a *Th$^{T2A-CreER}$*; *Avil^{FlpO}*; *ROSA26$^{DR-Matrix-dAPEX2}$* animal treated with tamoxifen at P14 to label C-LTMRs. Asterisks: labeled C-LTMR terminals. Arrowheads: synapses made by labeled C-LTMRs. n = 2 animals and experiments.

(**d**) EM images from an *Slc32a1$^{IRES-Cre}$*; *ROSA26$^{LSL-ER-dAPEX2}$* animal. Asterisks: labeled neurons. (Left) A dendrite of a cortical inhibitory interneuron. Arrowheads: synapses received by the labeled inhibitory interneuron. (Middle) A dendrite of a spinal cord dorsal horn inhibitory interneuron. Arrowhead: synapse received by the labeled inhibitory interneuron. (Right) Dendrites of striatal inhibitory neurons. Arrowhead: synapse received by a labeled inhibitory neuron. n = 2 animals and experiments.

Scale bars: **a**: (Left) 100 μm, (Middle and Right) 0.5 μm, **b**: (Left) 100 μm, (Middle and Right) 0.5 μm, **c, d**: 0.5 μm.

Table 1.

List of AAV constructs

AAV Construct	Recombinase Control	Addgene Plasmid #
pAAV-dAPEX2	None (constitutive)	117173
pAAV-DIO-dAPEX2	Cre-dependent	117174
pAAV-FDIO-dAPEX2	Flp-dependent	117175
pAAV-Matrix-dAPEX2	None (constitutive)	117176
pAAV-DIO-Matrix-dAPEX2	Cre-dependent	117177
pAAV-FDIO-Matrix-dAPEX2	Flp-dependent	117178
pAAV-IMS-dAPEX2	None (constitutive)	117179
pAAV-DIO-IMS-dAPEX2	Cre-dependent	117180
pAAV-FDIO-IMS-dAPEX2	Flp-dependent	117181
pAAV-ER-dAPEX2	None (constitutive)	117182
pAAV-DIO-ER-dAPEX2	Cre-dependent	117183
pAAV-FDIO-ER-dAPEX2	Flp-dependent	117184
pAAV-SV-HRP	None (constitutive)	117185
pAAV-DIO-SV-HRP	Cre-dependent	117186
pAAV-FDIO-SV-HRP	Flp-dependent	117187

Table 2.

List of mouse reporter lines

Mouse Line	Recombinase Control	JAX Stock #
ROSA26^DR-Matrix-dAPEX2	Cre-and-Flp-dual-dependent	032764
ROSA26^LSL-Matrix-dAPEX2	Cre-dependent	032765
ROSA26^FSF-Matrix-dAPEX2	Flp-dependent	032766
ROSA26^DR-ER-dAPEX2	Cre-and-Flp-dual-dependent	032767
ROSA26^LSL-ER-dAPEX2	Cre-dependent	032768
ROSA26^FSF-ER-dAPEX2	Flp-dependent	032769